

An innovative way of etching MoS₂: Characterization and mechanistic investigation

Yuan Huang^{1,2,3,†}, Jing Wu^{2,3,†}, Xiangfan Xu^{2,3}, Yuda Ho^{2,3}, Guangxin Ni^{2,3}, Qiang Zou¹, Gavin Kok Wai Koon^{2,3}, Weijie Zhao^{2,3,4}, A. H. Castro Neto^{2,3,6}, Goki Eda^{2,3,4}, Chengmin Shen¹ and Barbaros Özyilmaz^{2,3,5,6*}

¹Beijing National Laboratory for Condensed Matter Physics, Institute of Physics, Chinese Academy of Sciences, Beijing, China 100190

²Department of Physics, 2 Science Drive 3, National University of Singapore, Singapore 117542

³Graphene Research Centre, 6 Science Drive 2, National University of Singapore, Singapore 117542

⁴Department of Chemistry, National University of Singapore, 6 Science Drive 2, Singapore 117546

⁵Nanocore, 4 Engineering Drive 3, National University of Singapore, Singapore 117576

⁶NUS Graduate School for Integrative Sciences and Engineering (NGS), Centre for Life Sciences (CeLS), 28 Medical Drive, Singapore 117456.

ABSTRACT

We report a systematic study of the etching of MoS₂ crystals by using XeF₂ as a gaseous reactant. By controlling the etching process, monolayer MoS₂ with uniform morphology can be obtained. The Raman and photoluminescence spectra of the resulting material were similar to those of exfoliated MoS₂. Utilizing this strategy, different patterns such as a Hall bar structure and a hexagonal array can be realized. Furthermore, the etching mechanism was studied by introducing graphene as an etching mask. We believe our technique opens an easy and controllable way of etching MoS₂, which can be used to fabricate complex nanostructures, such as nanoribbons, quantum dots and transistor structures. This etching process using XeF₂ can also be extended to other interesting two-dimensional crystals.

* Address correspondence to Barbaros Özyilmaz, barbaros@nus.edu.sg

†These two authors made an equal contribution to the work.

Two-dimensional (2D) crystals such as boron nitride (BN), bismuth telluride (Bi_2Te_3) and tungsten disulfide (WS_2) have attracted much attention due to their unique properties when exfoliated from the corresponding bulk 3D materials [1–4]. Graphene is by far the most studied 2D crystal because of its outstanding optical, mechanical, thermal and electronic properties [5–10]. However, pristine graphene does not have a band gap, which poses a major problem for its practical applications in high-performance field-effect transistors (FETs). Band gap engineering via nanoribbons or strain engineering brings about a deterioration of the unique transport properties in graphene [11, 12, 13]. Thus, searching for other 2D materials with suitable band gap is an important aspect from both scientific and application points of view.

MoS_2 is an indirect gap semiconductor with a 1.2 eV bandgap in its bulk form; single layer MoS_2 , on the other hand, is a direct gap semiconductor with a 1.8 eV bandgap [14]. The indirect-to-direct transition arises from quantum confinement effects as thickness decreases [15], which also results in an enhancement of the photoluminescence of monolayer MoS_2 [16]. A single layer MoS_2 transistor with a room temperature current on/off ratio as high as 1×10^8 and ultralow standby energy dissipation has been reported [17], which makes it a promising candidate for use in semiconductor nanoelectronic devices. The excellent mechanical and optical properties of MoS_2 also make it a material [18, 19, 20], which can be used in applications where flexibility and transparency are required.

Currently, most MoS_2 devices have been made by using exfoliated flakes directly. This can be attributed to the chemical and physical properties of MoS_2 , which make it impossible to react with common acids (such as hydrochloric acid, nitric acid and sulphuric acid) and bases (KOH, and NaOH) at room temperature [21, 22]. However,

the ability to etch MoS₂ monolayer to give different geometries is critical for both fundamental physics studies, i.e., spin-Hall & spin-valley exploration [23] and also its potential applications. Thus, a new route to define sophisticated structures of MoS₂ is in high demand.

In this paper, we report a chemical dry-etching and patterning method for MoS₂ by using XeF₂ as a gaseous reactant. Atomic force microscopy (AFM) was used to study the morphology before and after etching, and the etching rate was also calculated by comparing the thickness change. Raman spectroscopy, as a powerful tool to analyze structural and doping information, was also employed to study the changes after etching. The photoluminescence (PL) spectra of single layer MoS₂ after etching and exfoliated single layer were compared. In order to gain a deeper insight into the etching mechanism, chemical vapor deposition (CVD) graphene was used as an etching mask. Combined with traditional micro-nanofabrication technology, where poly (methyl methacrylate) (PMMA) was used as etching mask after electron beam lithography patterning, we successfully obtained a hexagonal MoS₂ pits array after transferring exfoliated graphene as a mask. This is the first systematic report of such etching of MoS₂, which will be useful for future investigations and applications.

MoS₂ and graphite crystal were purchased from RS Components. Single layer CVD graphene grown on copper foil was supplied by Samsung Company. XeF₂ with purity of 99.9% was used as etching gas in our experiments. An optical microscope (Zeiss imager. A 1m, RIC Facility) was used to image MoS₂ flakes. The etching process was carried out in a xenon difluoride etching system (e1 Mod, XACTIX). Morphologies of MoS₂ samples were examined by AFM (Dimension FastScan, Bruker). The Raman spectra and mappings were collected by using a Raman Microscope (Alpha 300R,

WITec). Photoluminescence spectra were observed by confocal fluorescence microscopy (NETGRA Spectra, NT-MDT). Few-layer exfoliated graphene was transferred onto MoS₂ flakes using a home-made transfer system. An e-beam lithography system (Nova NanoSEM 50, FEI Corp.) and a reactive ion etching system (VITA-MINI) were used for patterning the array of graphene holes.

MoS₂ multilayer flakes were obtained by mechanical exfoliation of bulk MoS₂ on a silicon substrate covered with 285 nm of thermally oxidized SiO₂. The substrate surface was cleaned in the RIE system before exfoliating flakes on it. When the system was pumped down to 1.0×10^{-3} Pa, oxygen gas was introduced at a flow rate of 20 sccm (sccm denotes cubic centimeters per minute at STP) to generate an oxygen plasma; the cleaning process takes 5 min at 20 W.

CVD graphene grown on copper foil was spin-coated with one layer of PMMA, after etching the copper foil with FeCl₂ solution, PMMA and graphene floated up. Thus we could easily transfer graphene onto the SiO₂ substrate with MoS₂ flakes. PMMA was removed by immersing in acetone for 3 hours.

In order to transfer exfoliated graphene onto MoS₂ flakes, we used the same mechanical transfer method as used in the fabrication of graphene/h-BN heterostructures [24]. We used an optical mask in this transfer process, which includes three layers: a glass slide, adhesive tape and one layer of PMMA. All of these three layers are transparent, so we could easily align the position of MoS₂ and graphene. After preparing the mask, we exfoliated graphene on top of PMMA, and then transferred few-layer graphene under an optical microscope.

Due to its highly oxidizing properties, XeF₂ is widely used in industry as an etching gas

for Si. Recently, XeF₂ has also been used as a powerful tool to modify the properties of graphene, such as conductivity, transparency and bandgap [25, 26, 27]. We chose XeF₂ for two reasons: firstly, due to its highly oxidizing properties, the gas reacts easily with MoS₂; secondly, the reaction by-products can be efficiently removed as gases, such as Xe, SF₆, F₂, and MoF₃ et al. The reaction can be given as follow:



This strong oxidation-reduction reaction produces a large amount of heat and the temperature of the MoS₂ flakes is like to increase as a consequence, thus resulting in a positive influence on the reaction rate. All the products of this reaction are gases at room temperature. So at the end of the etching we can get very clean interface on our test samples.

The optical contrast on the substrate is sufficient to identify MoS₂ flakes with thickness down to a monolayer [17]. Figure 1a shows an optical image of a multilayered MoS₂ flake on Si/SiO₂ substrate. Figure 1b shows the same flake as in Fig. 1a after the etching process. The red zone marked in Fig. 1a was completely etched, whilst the remainder of the flakes remained due to their higher thickness.

The AFM images of one MoS₂ flake were also acquired on a 200 × 200 nm² scan window, and are shown in Figs. 1c and 1d. As clearly seen in these two images, the surface morphology of this flake changed considerably after etching, and the root-mean-square (rms) surface roughness changed from 0.07 nm to 0.9 nm, which is in consistent with a previous report by Castellanos-Gomez et al. [28]. There are two possible reasons for this result. Firstly, the reaction might not be uniform on the surface because of some molecular adsorption and traces of un-removed MoS₂. It may also originate from the microstructure of MoS₂, whereby due to the sandwich structure S–Mo–S, the reaction

rates of S layers and Mo layers might be different, thus causing an etching fluctuation.

In this study, all the etching experiments were conducted at room temperature. Higher pressures or longer times produced thinner flakes. Etching rate is very important for precise control of the etching thickness. In order to measure the etching rate, we prepared 24 samples at different etching times, and selected two different flakes in each sample for testing. The thickness of each flake was measured by AFM before and after etching. Figures S-1a and S1-b in the Electronic Supplementary Material (ESM) show the AFM images and height profile of the same MoS₂ flake, from which it can be seen that the thickness decreased by 18.8 nm after etching. The variation of etched thickness versus time can be clearly seen in Fig. 2; there was no obvious thickness change in the first 20 s, and the etching rate then accelerated after 30 s.

Although mechanical exfoliation methods have proven to be effective in giving high quality single or few layers MoS₂, most of the samples are very small and the yield is hard to control. Therefore, future research and applications require the development of a new procedure to precisely control the quality and layer numbers. Laser-thinning of MoS₂ has been reported as an effective way to get single-layer 2D crystals from multilayered flakes [28], but this method is still hard to control. After we calculated the etching rate, we also tried to obtain single layer MoS₂ by XeF₂ etching. Figure 3a shows an optical image of a multilayered MoS₂ flake on the substrate. As seen clearly in the marked zone, the flake was a golden color. Figure 3b shows the optical image of the same flake after XeF₂ etching for 120 s at 1 torr; one part of the marked zone became blue and one part became more transparent. AFM measurements showed that the edge thickness was 0.9 nm (Fig. S-2 in the ESM), which is consistent with a previous report [28].

Raman spectroscopy is a sensitive characterization method that has been widely used to study 2D materials [29, 30, 31]. For graphene, the layer numbers, defects, strain and substrate effects can be easily determined from its Raman spectrum [29, 32]. Lee et al. reported a systematic study of the Raman spectrum of MoS₂; the Raman shift changed gradually as the layer number increased [33]. The intrinsic peaks of MoS₂, E_{12g} and A_{1g} occur at around 380 and 400 cm⁻¹ respectively. The frequency difference between the two most prominent peaks can be used as a direct proof of layer number; however the difference remains almost the same for layer number larger than 5. In Fig. 3c, we compare the difference in Raman spectra before and after etching. The two peaks of thick MoS₂ flakes are located at 384 and 409 cm⁻¹, with the separation between the two peaks being about 25 cm⁻¹. As the thickness decreased after XeF₂ treatment, the frequency difference between the two peaks decreased to 19 cm⁻¹. The frequency difference between E_{12g} and A_{1g} is the same as for exfoliated monolayer MoS₂. This means that the intrinsic vibration mode did not change significantly even after etching. Spatial maps (5 μm × 5 μm) of the Raman frequency of modes E_{12g} and A_{1g} are compared in Fig. S-3 (in the ESM). Due to the transition from an indirect to a direct-bandgap semiconductor, single layer MoS₂ exhibits a unique signature in its photoluminescence spectrum. In Fig. 3d, we compare the PL spectrum of the etched single layer and one exfoliated single layer sample. The exfoliated single layer sample has two PL peaks at 670 nm and 619 nm, consistent with previous reports [34]. These two peaks are due to the direct excitonic transitions at the Brillouin zone K point [35]. The PL spectrum of the etched single layer proves that the etched single layer MoS₂ also retains the large intrinsic direct bandgap. However the intensity of the etched sample is larger than that of the pristine sample and the dominant peak at 663 nm, shows a blue shift which indicates a larger bandgap. The mechanism of this effect is still unknown, but it may

arise from the quantum confinement effects as the thickness decreases. In addition, the exfoliated monolayer retains the S–Mo–S sandwich structure, but the etching-thinned monolayer sample could even break up the three-layer unit and make it into a thinner structure.

The etching process is closely related to the interaction between the bottom layer and the SiO₂ substrate. The reaction is an exothermic process, and elevated temperature can accelerate the reaction rate, such that the etching rate becomes faster as time increases as shown in Fig. 2. Because of the weak interlayer coupling between the MoS₂ layers, the heat cannot be easily dissipated to the surroundings during reaction. The bottom layer, however, remains due to the substrate effect. Similar effects have also been reported by other groups [28].

The fabrication of devices with different structures is critical for studying the intrinsic properties of 2D materials, such as Hall bar [7], FET [17, 36] and quantum dot devices [37]. By combining traditional electron beam lithography (EBL) and our etching method, we successfully fabricated some devices and patterns (see Fig. S-4 in the ESM). In these experiments, exfoliated MoS₂ flakes were put onto a SiO₂ substrate, and then one layer of PMMA was spin-coated on the chip. After EBL exposure and development, we obtained different patterns covered by PMMA. The patterned sample was put into the chamber and etched for 4 minutes at 1 torr pressure of XeF₂. Although etching with these parameters could completely remove MoS₂ flakes with a thickness less than 300 nm, the edge of the etched MoS₂ flake was still very sharp (Fig. S-4c in the ESM). This can be explained by forming one layer of PMMA film at the edge of MoS₂, because the heat during the reaction could make PMMA around the exposed area melt and cover the edge, and in this case the reaction will stop at the edge. Many groups have reported

the physical properties of XeF₂-fluorinated graphene. Even though the properties and functionalities can change during the fluorination process, the 2D structure can be retained after fluorination [25, 26, 27]. This means graphene can be used as an etching mask for many materials, such as Si, SiO₂ and MoS₂. In order to study the etching mechanism, the stack of monolayer CVD graphene and MoS₂ flakes is etched for 3 minutes at 1 torr, as shown in Fig. 4a. Interestingly, from the AFM image we find that there are some hexagonal pits on each flake. As shown in Fig. 4c, there is a hole in the center of the hexagonal pits (Fig. 4d). The reason for this is that the many defects in CVD graphene provide reaction centers and the reaction by-products were removed as gas, while the covered area could be gradually etched from the defect centers. This means that the defects in CVD graphene can be easily detected in this way.

Considering that the position and amount of defects in CVD graphene is hard to control, exfoliated few-layer graphene is chosen as a mask for further study. Exfoliated graphene is an almost perfect 2D crystal, so the defects can be easily designed by using EBL and oxygen plasma. Figure 4b shows the optical image of the hexagonal pits array; the etched hole of graphene can be clearly seen at the center of every hexagonal trench and these trenches are aligned to each other. The main difference between PMMA and graphene as an etching mask is that graphene with its high thermal conductivity and stability does not form an insulating layer, which is why we could obtain hexagonal pits under graphene.

Considering that XeF₂ molecules are the only reactive species in this process, and only the presence of point defects could induce hexagonal pits, we build a simple model to explain the etching mechanism. In the microstructure of monolayer MoS₂, each Mo atom is bonded to six S atoms, and each S atom is bonded to three Mo atoms (Fig. 5a).

Figure 5b shows the top view of a monolayer MoS₂ atomic structure, assuming that this monolayer MoS₂ was covered by CVD graphene with only one point defect in the center of the graphene. After we remove one S atom from the top layer (Fig. 5c), three Mo atoms in the middle layer and one S atom will be exposed to XeF₂, and they will become more active than the other atoms in the whole crystal. Then XeF₂ will selectively remove the four atoms, and in this case the first hexagonal hole can be observed (Fig. 5d). Following this, the exposed atoms in MoS₂ crystal will be removed in sequence, as shown in Figs. 5e–5f, resulting in hexagonal pits after etching.

First-principles computation predicts that zigzag MoS₂ nanoribbons show ferromagnetic and metallic behavior, irrespective of the ribbon width and thickness, while the armchair nanoribbons are nonmagnetic and semiconducting [38, 39]. Until now, there has been no experimental report of the properties of zigzag or armchair MoS₂ nanoribbons. As shown in our model, all the edges in the hexagonal pits are zigzag. This means zigzag MoS₂ nanoribbons can be fabricated by controlling the position of graphene defects and etching parameters, and its ferromagnetic properties could be realized on multilayered MoS₂ flakes.

Conclusions

We have discovered a strategy for etching MoS₂ using XeF₂ as a reaction gas. The morphology change and etching parameters were systematically studied. By controlling the etching process, monolayer MoS₂ with high quality can be realized. Raman and photoluminescence spectra demonstrated that the etched flakes are as regular as the pristine ones. By using PMMA as an etching mask, we successfully combined micro-

fabrication technology with this etching method to obtain different geometric structures. In order to study the etching mechanism, graphene was employed as an etching mask, and the etching process was clearly illustrated by a simple model. The model indicates that zigzag MoS₂ nanoribbons can be fabricated by optimizing the etching process. Assuming that a wafer-scale single-crystal multilayered MoS₂ is available, this etching method could provide a useful tool for the fabrication of large-area single layer MoS₂ for integrated devices. Thus, a road can be paved for future fundamental studies and integrated nanodevices based on the method reported here.

Acknowledgements

This work was supported by the NRF-CRP award "Novel 2D materials with tailored properties: beyond graphene" (R-144-000-295-281), the Singapore National Research Foundation Fellowship award NRF-RF2008-07, Singapore Millennium Foundation (SMF)-NUS Research Horizons Award 2009 (R-144-001-271-592, R-144-001-271-646), and the National Basic Research Program of China (973 Program, Grants No. 2013CB933604, No. 2011CB932703).

References

- [1]. Coleman, J. N.; Lotya, M.; O'Neill, A.; Bergin, S. D.; King, P. J.; Khan, U.; Young, K.; Gaucher, A.; De, S.; Smith, R. J.. Two-dimensional nanosheets produced by liquid exfoliation of layered materials. *Science* **2011**, *331*, 568–571.
- [2]. Steinberg, H.; Gardner, D. R.; Lee, Y. S.; Jarillo-Herrero, P. Surface state transport and ambipolar electric field effect in Bi₂Se₃ nanodevices. *Nano Lett.* **2010**, *10*, 5032–5036.
- [3]. Ramakrishna Matte, H. S. S.; Gomathi, A.; Manna, A. K.; Late, D. J.; Datta, R.; Pati, S. K.; Rao, C. N. R. MoS₂ and WS₂ analogues of graphene. *Angew. Chem.* **2010**, *122*, 4153–4156.
- [4]. Teweldebrhan, D.; Goyal, V.; Balandin, A. A. Exfoliation and characterization of bismuth telluride atomic quintuples and quasi-two-dimensional crystals. *Nano Lett.* **2010**, *10*, 1209–1218.

- [5]. Lee, C.; Wei, X.; Kysar, J. W.; Hone, J. Measurement of the elastic properties and intrinsic strength of monolayer graphene. *Science* **2008**, *321*, 385–388.
- [6]. Ni, G. X.; Zheng, Y.; Bae, S.; Tan, C. Y.; Kahya, O.; Wu, J.; Hong, B. H.; Yao, K.; Özyilmaz, B. Graphene-ferroelectric hybrid structure for flexible transparent electrodes. *ACS Nano* **2012**, *6*, 3935–3942.
- [7]. Novoselov, K.; Geim, A.; Morozov, S.; Jiang, D.; Grigorieva, M. I. K. I. V.; Dubonos, S.; Firsov, A. Two-dimensional gas of massless Dirac fermions in graphene. *Nature* **2005**, *438*, 197–200.
- [8]. Yang, R.; Zhang, L. C.; Wang, Y.; Shi, Z. W.; Shi, D. X.; Gao, H. J.; Wang, E. G.; Zhang, G. Y. An anisotropic etching effect in the graphene basal plane. *Adv. Mater.* **2010**, *22*, 4014–4019.
- [9]. Castro Neto, A. H.; Guinea, F.; Peres, N. M. R.; Novoselov, K. S.; Geim, A. K. The electronic properties of graphene. *Rev. Mod. Phys.* **2009**, *81*, 109–162.
- [10]. Shi, Z. W.; Yang, R.; Zhang, L. C.; Wang, Y.; Liu, D. H.; Shi, D. X.; Wang, E. G.; Zhang, G. Y. Patterning graphene with zigzag edges by self-aligned anisotropic etching. *Adv. Mater.* **2011**, *23*, 3061–3065.
- [11]. Lu, Y. H.; Feng, Y. P. Band-gap engineering with hybrid graphene-graphene nanoribbons. *J. Phys. Chem. C* **2009**, *113*, 20841–20844.
- [12]. Balog, R.; Jørgensen, B.; Nilsson, L.; Andersen, M.; Rienks, E.; Bianchi, M.; Fanetti, M.; Lægsgaard, E.; Baraldi, A.; Lizzit, S. et al. Bandgap opening in graphene induced by patterned hydrogen adsorption. *Nat. Mater.* **2010**, *9*, 315–319.
- [13]. Jiao, L. Y.; Zhang, L.; Wang, X. R.; Diankov, G.; Dai, H. J. Narrow graphene nanoribbons from carbon nanotubes. *Nature* **2009**, *458*, 877–880.
- [14]. Mak, K. F.; Lee, C.; Hone, J.; Shan, J.; Heinz, T. F. Atomically thin MoS₂: A new direct-gap semiconductor. *Phys. Rev. Lett.* **2010**, *105*, 136805.
- [15]. Kuc, A.; Zibouche, N.; Heine, T. Influence of quantum confinement on the electronic structure of the transition metal sulfide TS₂. *Phys. Rev. B* **2011**, *83*, 245213.
- [16]. Korn, T.; Heydrich, S.; Hirmer, M.; Schmutzler, J.; Schüller, C. Low-temperature photocarrier dynamics in monolayer MoS₂. *Appl. Phys. Lett.* **2011**, *99*, 102109.
- [17]. Radisavljevic, B.; Radenovic, A.; Brivio, J.; Giacometti, V.; Kis, A. Single-layer MoS₂ transistors. *Nat. Nanotechnol.* **2011**, *6*, 147–150.
- [18]. Bertolazzi, S.; Brivio, J.; Kis, A. Stretching and breaking of ultrathin MoS₂. *ACS Nano* **2011**, *5*, 9703–9709.
- [19]. Castellanos-Gomez, A.; Poot, M.; Steele, G. A.; van der Zant, H. S. J.; Agraït, N.; Rubio-Bollinger, G. Elastic properties of freely suspended MoS₂ nanosheets. *Adv. Mater.* **2012**, *24*, 772–775.
- [20]. Fortin, E.; Sears, W. M. Photovoltaic effect and optical absorption in MoS₂. *J. Phys. Chem. Solids* **1982**, *43*, 881–884.
- [21]. Chen, Z.; Cummins, D.; Reinecke, B. N.; Clark, E.; Sunkara, M. K.; Jaramillo, T. F. Core-shell-MoO₃-MoS₂ nanowires for hydrogen evolution: A functional design for electrocatalytic materials. *Nano Lett.* **2011**, *11*, 4168–4175.
- [22]. Miyake, K.; Shigekawa, H. Surface structures of layered compounds treated with alkali-metal hydroxide solutions studied by scanning tunneling microscopy. *Synth. Met.* **1995**, *71*, 1753–1754.
- [23]. Xiao, D.; Liu, G. B.; Feng, W. X.; Xu, X. D.; Yao, W. Coupled spin and valley physics in monolayers of MoS₂ and other group-VI dichalcogenides. *Phys. Rev. Lett.* **2012**, *108*,

196802.

- [24]. Zomer, P. J.; Dash, S. P.; Tombros, N.; van Wees, B. J. A new transfer technique for high mobility graphene devices on commercially available hexagonal boron nitride. *Appl. Phys. Lett.* **2011**, *99*, 232104.
- [25]. Robinson, J. T.; Burgess, J. S.; Junkermeier, C. E.; Badescu, S. C.; Reinecke, T. L.; Perkins, F. K.; Zalalutdniov, M. K.; Baldwin, J. W.; Culbertson, J. C.; Sheehan, P. E. et al. Properties of fluorinated graphene films. *Nano Lett.* **2010**, *10*, 3001–3005.
- [26]. Withers, F.; Dubois, M.; Savchenko, A. K. Electron properties of fluorinated single-layer graphene transistors. *Phys. Rev. B* **2010**, *82*, 073403.
- [27]. Ribas, M. A.; Singh, A. K.; Sorokin, P. B.; Yakobson, B. I. Patterning nanoroads and quantum dots on fluorinated graphene. *Nano Res.* **2011**, *4*, 143–152.
- [28]. Castellanos-Gomez, A.; Barkelid, M.; Goossens, A. M.; Calado, V. E.; van der Zant, H. S. J.; Steele, G. A. Laser-thinning of MoS₂: On demand generation of a single-layer semiconductor. *Nano Lett.* **2012**, *12*, 3187–3192.
- [29]. Ferrari, A. C.; Meyer, J. C.; Scardaci, V.; Casiraghi, C.; Lazzeri, M.; Mauri, F.; Piscanec, S.; Jiang, D.; Novoselov, K. S.; Roth, S.; Geim, A. K. Raman spectrum of graphene and graphene layers. *Phys. Rev. Lett.* **2006**, *97*, 187401.
- [30]. Gorbachev, R. V.; Riaz, I.; Nair, R. R.; Jalil, R.; Britnell, L.; Belle, B. D.; Hill, E. W.; Novoselov, K. S.; Watanabe, K.; Taniguchi, T.; Geim, A. K.; Blake, P. Hunting for monolayer boron nitride: Optical and Raman signatures. *Small* **2011**, *7*, 465–468.
- [31]. Frey, G. L.; Tenne, R.; Matthews, M. J.; Dresselhaus, M. S.; Dresselhaus, G. Raman and resonance Raman investigation of MoS₂ nanoparticles. *Phys. Rev. B* **1999**, *60*, 2883–2892.
- [32]. Calizo, I.; Balandin, A. A.; Bao, W.; Miao, F.; Lau, C. N. Temperature dependence of the Raman spectra of graphene and graphene multilayers. *Nano Lett.* **2007**, *7*, 2645–2649.
- [33]. Lee, C.; Yan, H.; Brus, L. E.; Heinz, T. F.; Hone, J.; Ryu, S. Anomalous lattice vibrations of single and Few-Layer MoS₂. *ACS Nano* **2010**, *4*, 2695–2700.
- [34]. Splendiani, A.; Sun, L.; Zhang, Y. B.; Li, T.; Kim, J.; Chim, C. Y.; Galli, G.; Wang, F. Emerging photoluminescence in monolayer MoS₂. *Nano Lett.* **2010**, *10*, 1271–1275.
- [35]. Coehoorn, R.; Haas, C.; de Groot, R. A. Electronic structure of MoSe₂, MoS₂, and WSe₂. II. The nature of the optical band gaps. *Phys. Rev. B* **1987**, *35*, 6203–6306.
- [36]. Ni, G. X.; Zheng, Y.; Bae, S.; Kim, H. R.; Pachoud, A.; Kim, Y. S.; Tan, C. L.; Im, D.; Ahn, J. H.; Hong, B. H.; Özyilmaz, B.; Quasi-Periodic Nanoripples in Graphene Grown by Chemical Vapor Deposition and Its Impact on Charge Transport. *ACS Nano* **2012**, *6*, 1158–1164.
- [37]. Silvestrov, P. G.; Efetov, K. B. Quantum dots in graphene. *Phys. Rev. Lett.* **2007**, *98*, 016802.
- [38]. Ataca, C.; Sahin, H.; Akturk, E.; Ciraci, S. Mechanical and electronic properties of MoS₂ nanoribbons and their defects. *J. Phys. Chem. C* **2011**, *115*, 3934–3941.
- [39]. Li, Y. F.; Zhou, Z.; Zhang, S. B.; Chen, Z. F. MoS₂ nanoribbons: High stability and unusual electronic and magnetic properties. *J. Am. Chem. Soc.* **2008**, *130*, 16739–16744.

Figure Caption

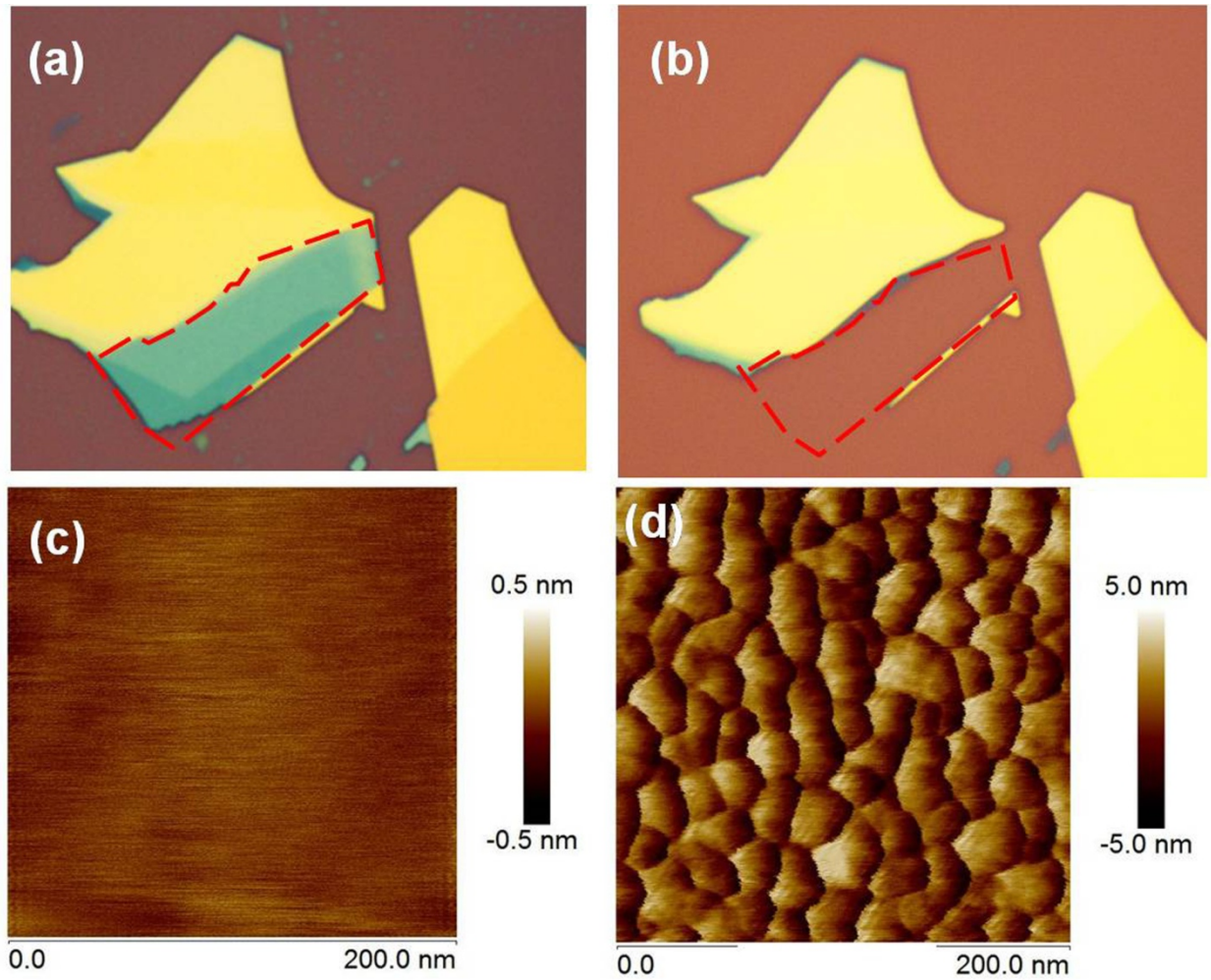


Figure 1 Optical and AFM images of a MoS₂ flake. (a) and (b) are the optical images before and after etching. (c) and (d) are the corresponding AFM images of the lower right corner flake in (a) and (b).

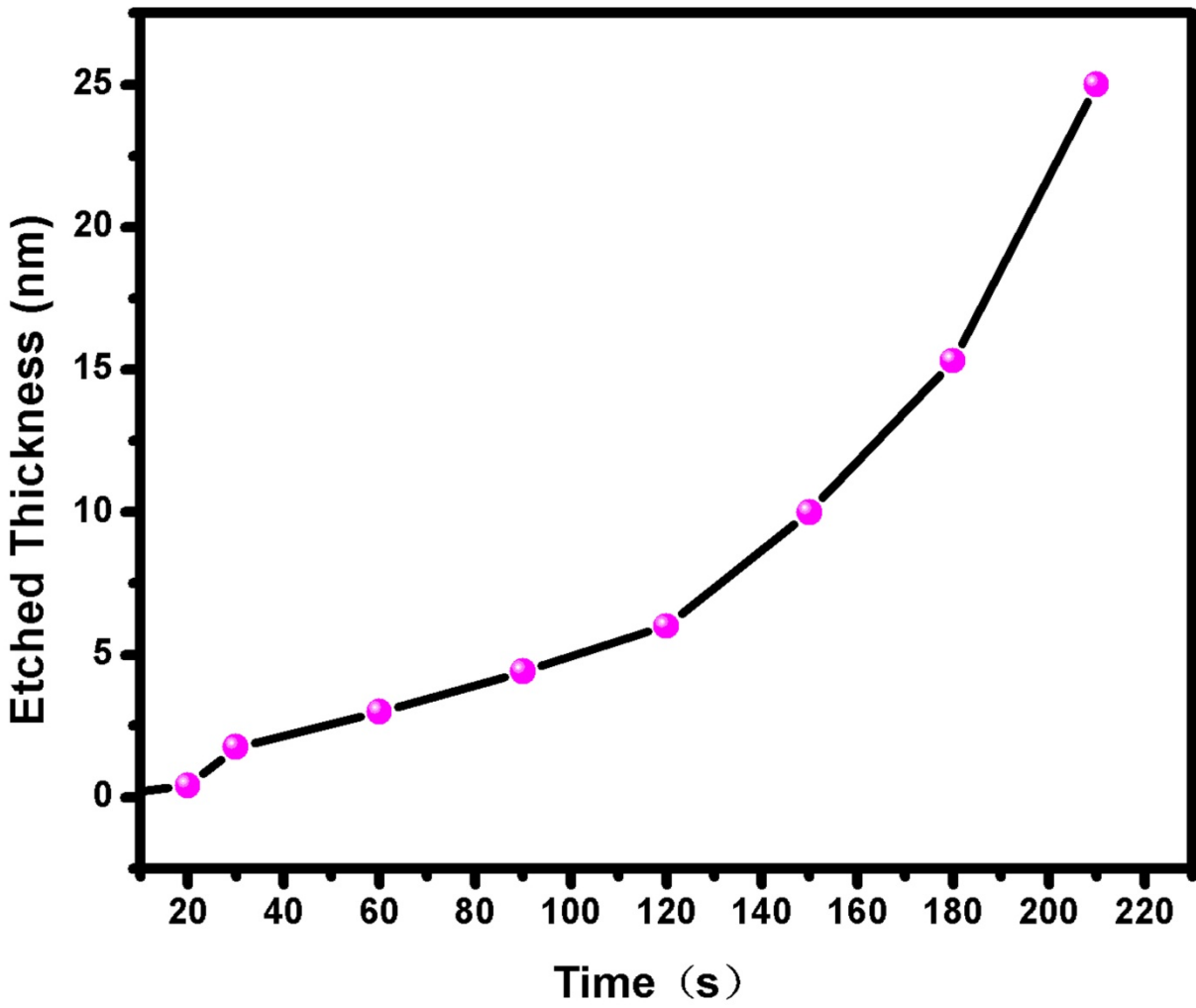


Figure 2 Thickness measurement and etching rate analysis. Plot of etched thickness vs. time for 12 samples (the pressure was 1 torr, and each point corresponds to two samples).

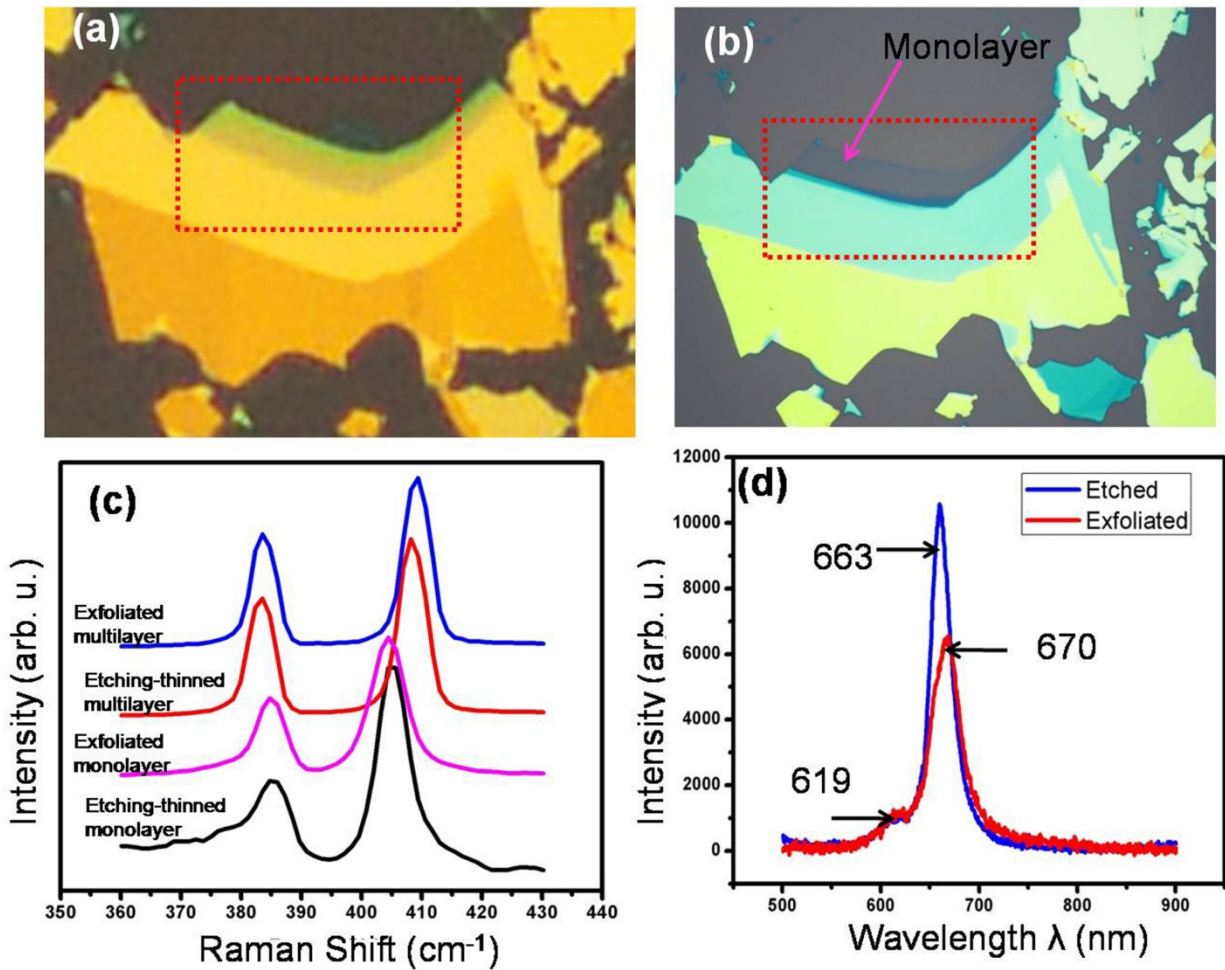


Figure 3 Optical images of an etching-thinned monolayer and its photoluminescence spectrum. (a) Optical image of MoS₂ before etching. (b) Optical image of the same flake after etching; monolayer MoS₂ can be clearly seen in the marked zone. (c) Raman spectra of the exfoliated multilayer and monolayer and the corresponding etching-thinned samples. (d) The photoluminescence spectra of etching-thinned monolayer and exfoliated monolayer samples.

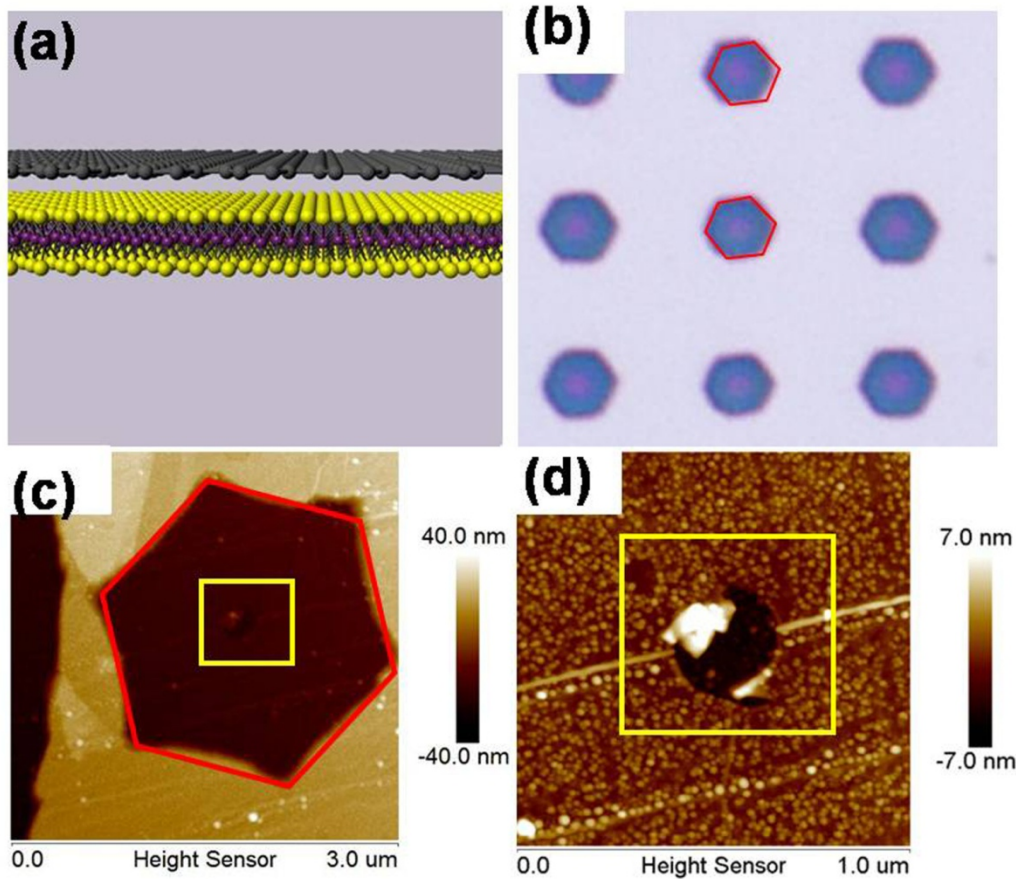


Figure 4 AFM and optical images of hexagonal pits. (a) Schematic image of a MoS₂ flake after covering one layer of graphene. (b) Optical image of hexagonal array: few layer graphene was put onto this MoS₂ flake, then a hole array was patterned by combining EBL and oxygen plasma before etching. Two of the hexagonal pits are marked with red curves. (c) AFM image of the hexagonal pit, where the edge and center of the hexagonal pit are marked with red and yellow curves, respectively. (d) The zoom-in AFM image of the center in (c), which originated from a point defect of CVD graphene.

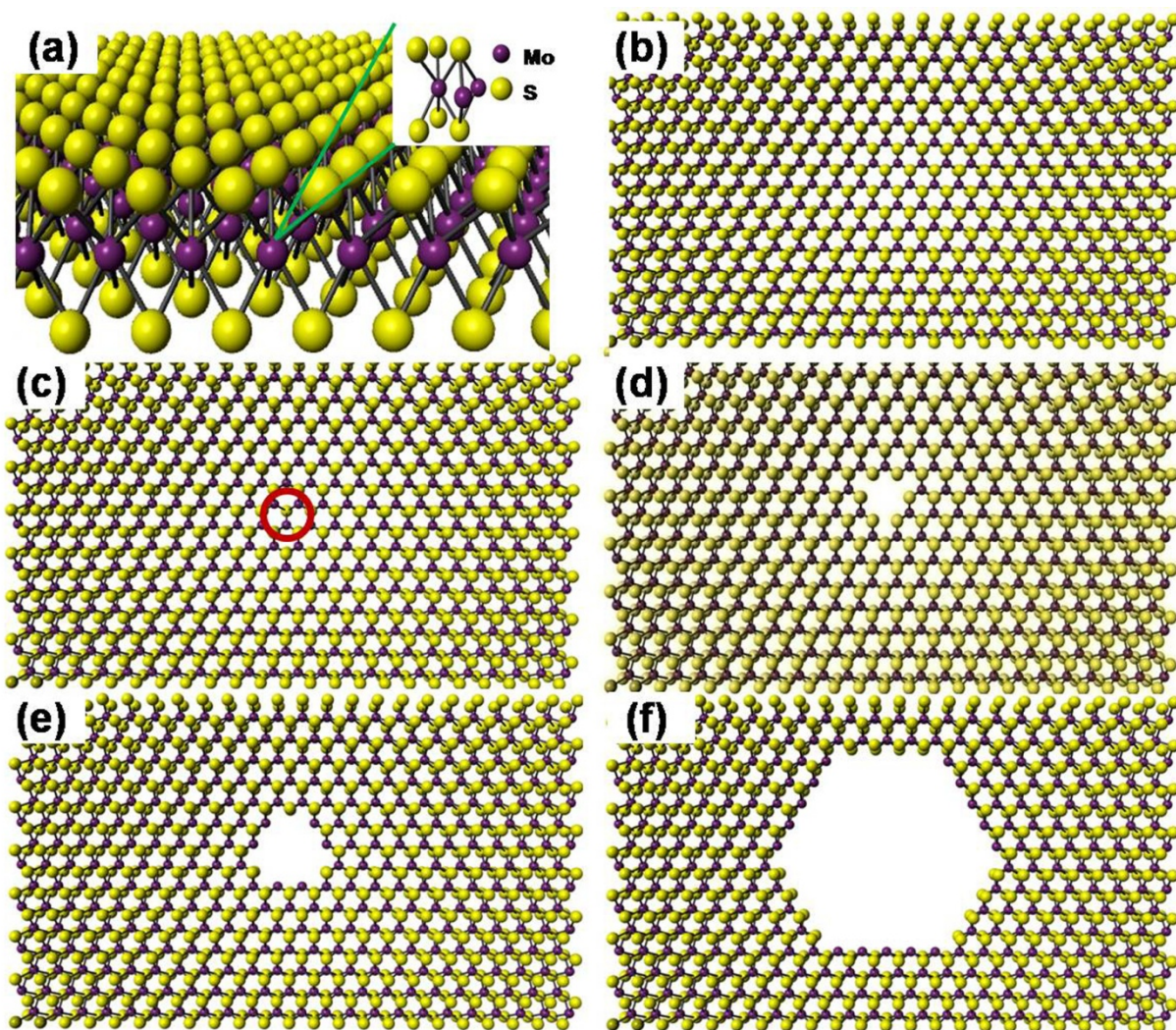


Figure 5 Schematic model of the atomic structure of monolayer MoS₂ and the etching mechanism. (a) Atomic structure of monolayer MoS₂, where the inset shows the unit cell of the crystal. (b) Top view of a monolayer MoS₂ crystal, assuming the crystal was covered by CVD graphene. (c) After removing one S atom on top from one point defect of graphene (see the marked zone), three Mo atoms with dangling bonds are exposed to XeF₂. (d) After removing three Mo atoms in the middle layer and one S atom at the bottom by XeF₂. (e) and (f) The hexagonal pit growing larger during the etching process.

Supplementary Material

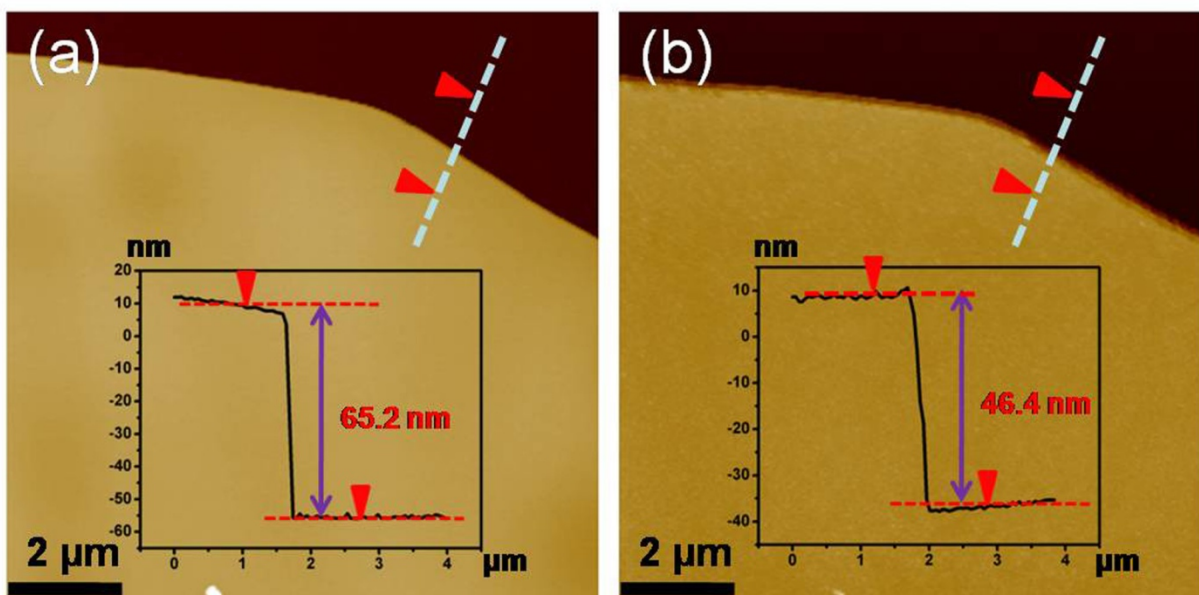


Figure S-1 AFM images of the same MoS₂ flake before and after etching, with height profiles shown in the insets. (a) The thickness of pristine exfoliated MoS₂ is 65.2 nm. (b) The thickness of this flake decreased to 46 nm after etching for 180 s at 1 torr. By comparing the thickness changes, the plot of $\Delta T_{\text{thickness}}$ vs. time can be acquired as shown in Fig. 2.

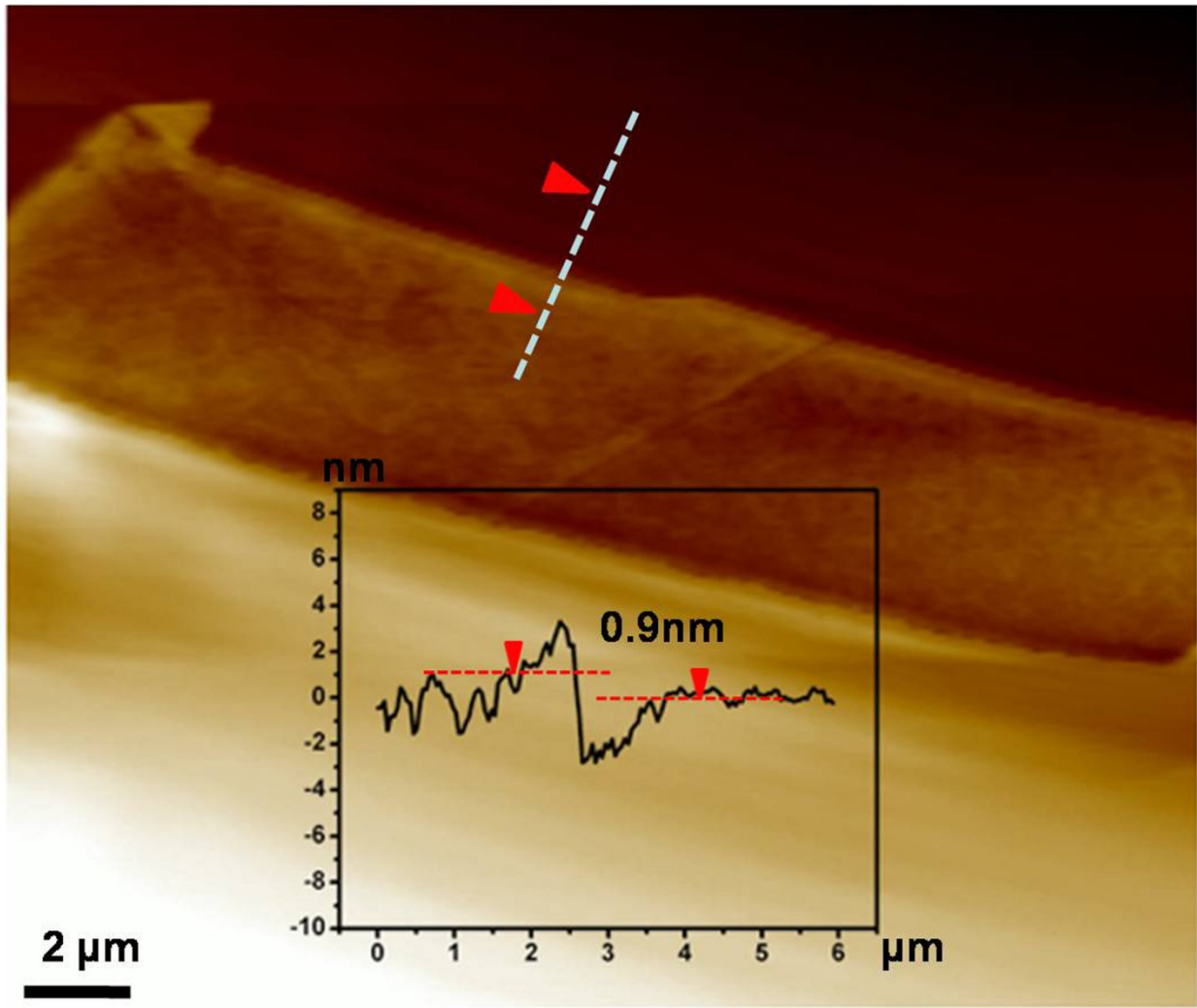


Figure S-2 AFM image of the etching-thinned monolayer MoS₂, which is the sample shown in Fig. 3. The height profile is shown in the inset.

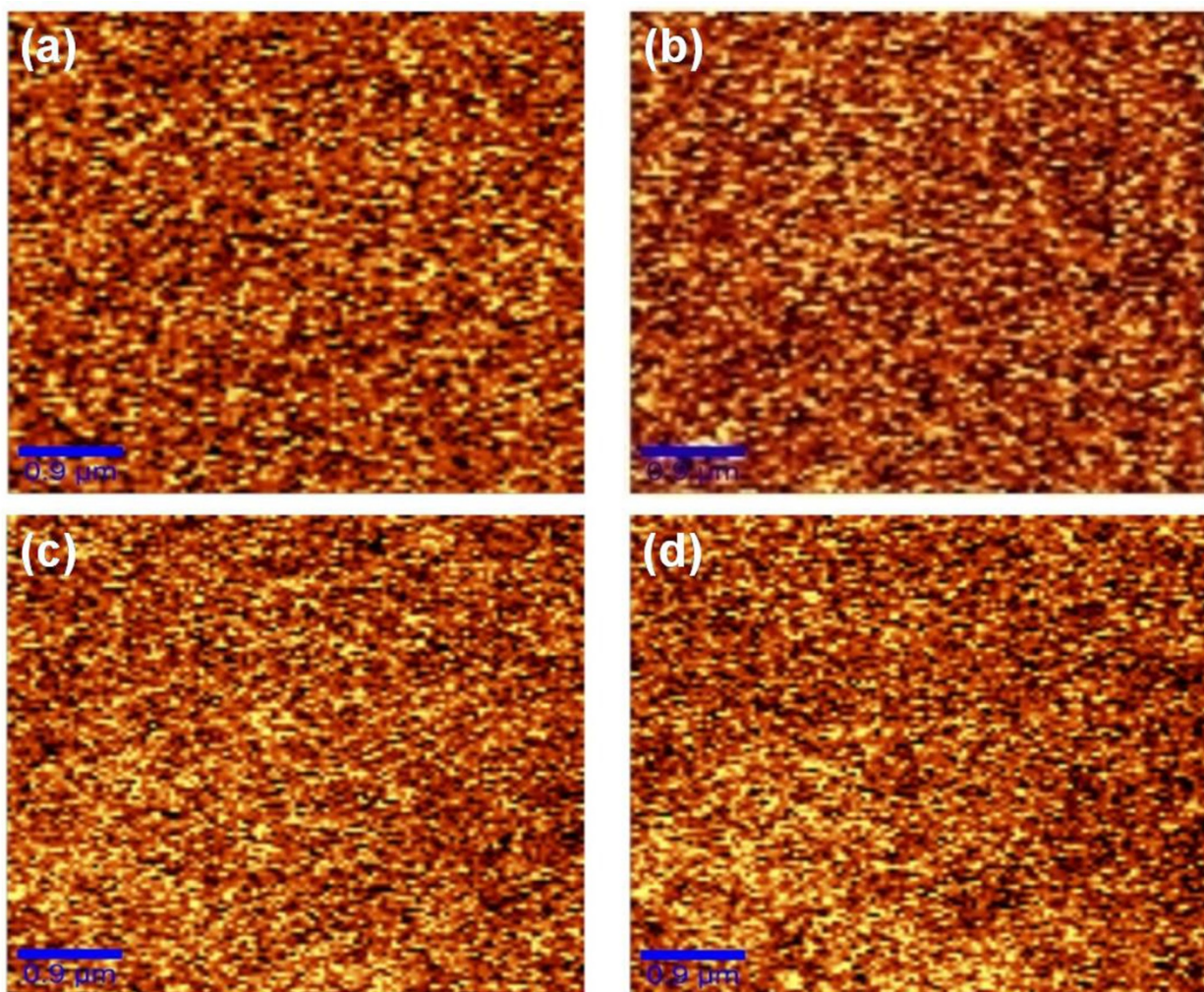


Figure S-3 Spatial maps ($5 \mu\text{m} \times 5 \mu\text{m}$) of Raman bands E_{2g}^1 (a, c) and A_{1g} (b, d) for multilayered MoS_2 . (a) and (b) are the spatial maps of an exfoliated MoS_2 flake, while (c) and (d) are the spatial maps of the same MoS_2 flake after etching.

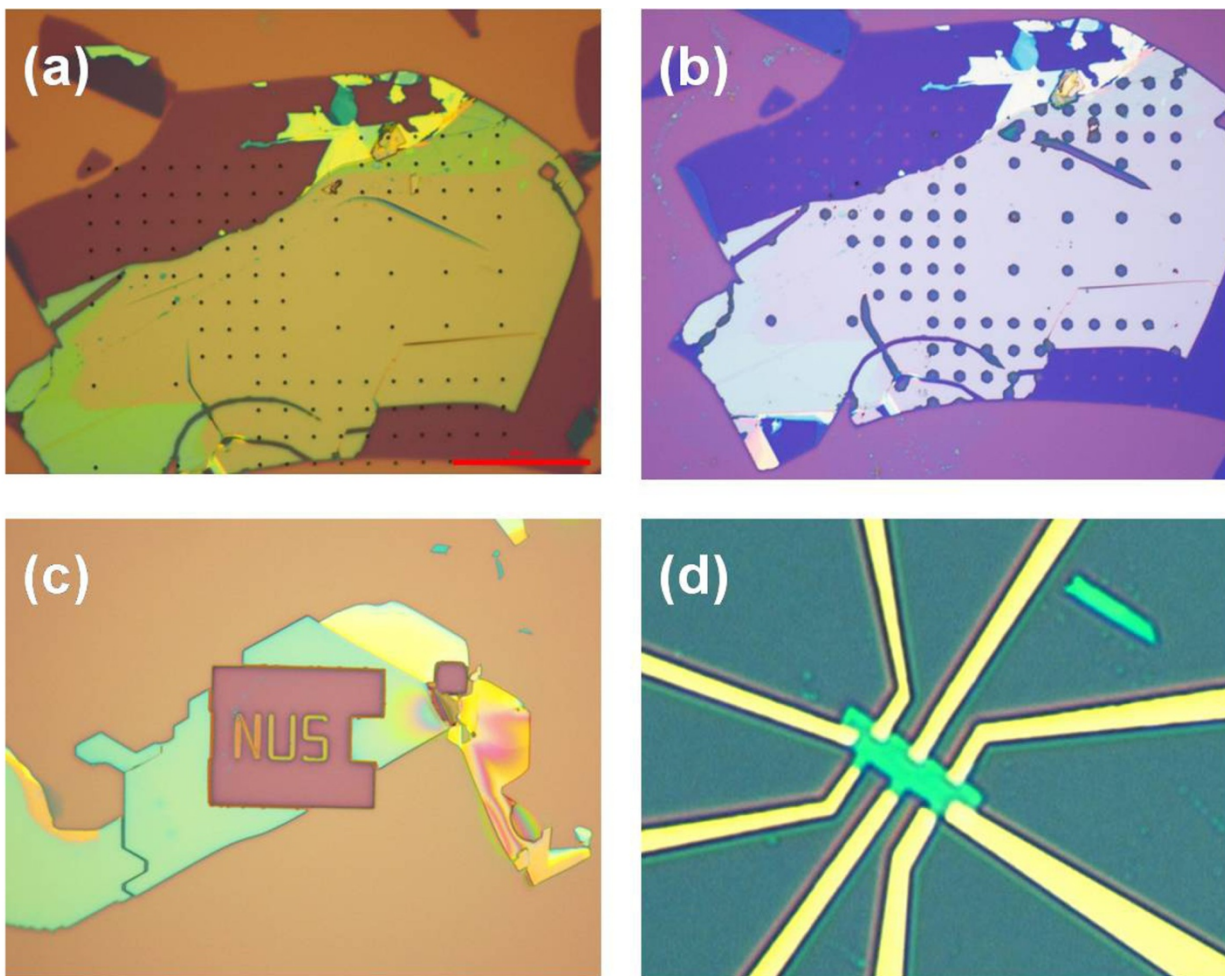


Figure S-4 Images of MoS₂ pattern and device. (a) Image of MoS₂ flake covered by few-layer exfoliated graphene. An array of holes were fabricated on few-layer graphene by e-beam lithography and oxygen-plasma etching. Hexagonal pits grown in an MoS₂ flake from graphene holes after XeF₂ etching, as shown in (b) and Fig. 4b. (c) Image of one pattern on an MoS₂ flake. (d) Image of an MoS₂ device fabricated after e-beam lithography and XeF₂ etching.